Composite Structures 323 (2023) 117452

Contents lists available at ScienceDirect

Composite Structures

journal homepage: www.elsevier.com/locate/compstruct

Improved ballistic limit velocity from filament-wound fibres as composite cover on ceramic tiles

Dennis B. Rahbek [a], Gwyn E. Roberson [b], Bernt B. Johnsen [a,*]

[a] Norwegian Defence Research Establishment (FFI), P.O. Box 25, NO-2027 Kjeller, Norway
[b] NFM Group AS, Glynitveien 15, NO-1400 Ski, Norway

ARTICLE INFO

Keywords:
Ballistic limit velocity
Composite cover
Manufacturing method
Alumina ceramic
Armour piercing projectile

ABSTRACT

Hard armour plates are used in body armour for protection against high-velocity threats. The strike face often consists of a single ceramic tile that is covered by a sheet material made of a high-tenacity fibre-composite material. During impact, the ceramic will fracture but at the same time cause erosion and fragmentation of the hard core of the projectile. The composite cover is there to improve the ballistic performance by partly maintaining the integrity of the fracturing ceramic. In this study, a new production method where glass fibre yarns were filament-wound around an alumina tile in a unidirectional 0°/90° lay-up, was investigated. Ballistic testing was conducted with a 7.62 mm armour piercing projectile. The new target design gave a remarkable increase in the V_{50} ballistic limit velocity by as much as 16% compared to a traditional design where a glass fibre fabric was wrapped around the tile. A higher degree of fragmentation of the projectile steel core after perforation was also observed. The high degree of fibre alignment in the filament-wound composite, as opposed to the more wavy fibres in the fabric, is believed to be the main reason for the higher ballistic performance.

1. Introduction

Modern solutions for light-weight ballistic protection of soldiers are made from combinations of different materials. In a military context, the materials are combined in such a way that the protection system is as light weight as possible, given the specific threat they are designed to protect against. This is to reduce burden and thus improve the mobility, endurance and comfort of the soldier. Hence, there is always a drive amongst armour manufacturers to implement new, more efficient materials that are coming into the market and to improve the manufacturing methods to be able to provide systems with improved performance.

The two main components in a typical body armour system are a soft ballistic panel and a hard armour plate [1–4]. The soft panel is made of high-performance ballistic fibres, as for example aramid and ultra-high molecular weight polyethylene (UHMWPE), that provide protection to the soldier from various types of relatively small primary and secondary fragments from indirect fire munitions, and in many cases handgun rounds. This is achieved from the fibres' ability to absorb and disperse the kinetic energy of the fragments or the bullets. The hard armour plate, on the other hand, gives protection against projectiles with higher kinetic energy, the most serious threat being high-velocity armour piercing (AP) rifle bullets. The hard armour plate typically consists of a monolithic, double-curved ceramic tile which is wrapped in a thin composite material. Additionally, at the back of the wrapped ceramic tile, there is a backing that is made from several layers of ballistic fibres. The hard armour plate can be designed to be used as a stand-alone plate, or more commonly, in conjunction with the soft panel.

The ceramic is commonly composed of alumina, silicon carbide or boron carbide and acts as the strike face in the hard armour plate. The composition of the ceramic is designed according to the expected threat level and the weight and cost requirements of the armour system. The main reason for using ceramics as the strike face is that they are very hard materials with a relatively low density. When an AP projectile impacts on the armour, the hard core of the projectile will be eroded at the tip and fragmentation of the core will occur. However, ceramics are brittle materials and they will fracture during impact due to the high stress loads thus causing the formation of radial cracks, cone cracks and fragmentation of the ceramic [5–10]. The comminuted ceramic that is formed in the area in front of the projectile then becomes less confined, resulting in lower resistance to penetration.

To improve the ballistic performance of the ceramic tile, it can be

* Corresponding author.
E-mail address: bernt.johnsen@ffi.no (B.B. Johnsen).

https://doi.org/10.1016/j.compstruct.2023.117452
Received 3 February 2023; Received in revised form 7 July 2023; Accepted 10 August 2023
Available online 15 August 2023

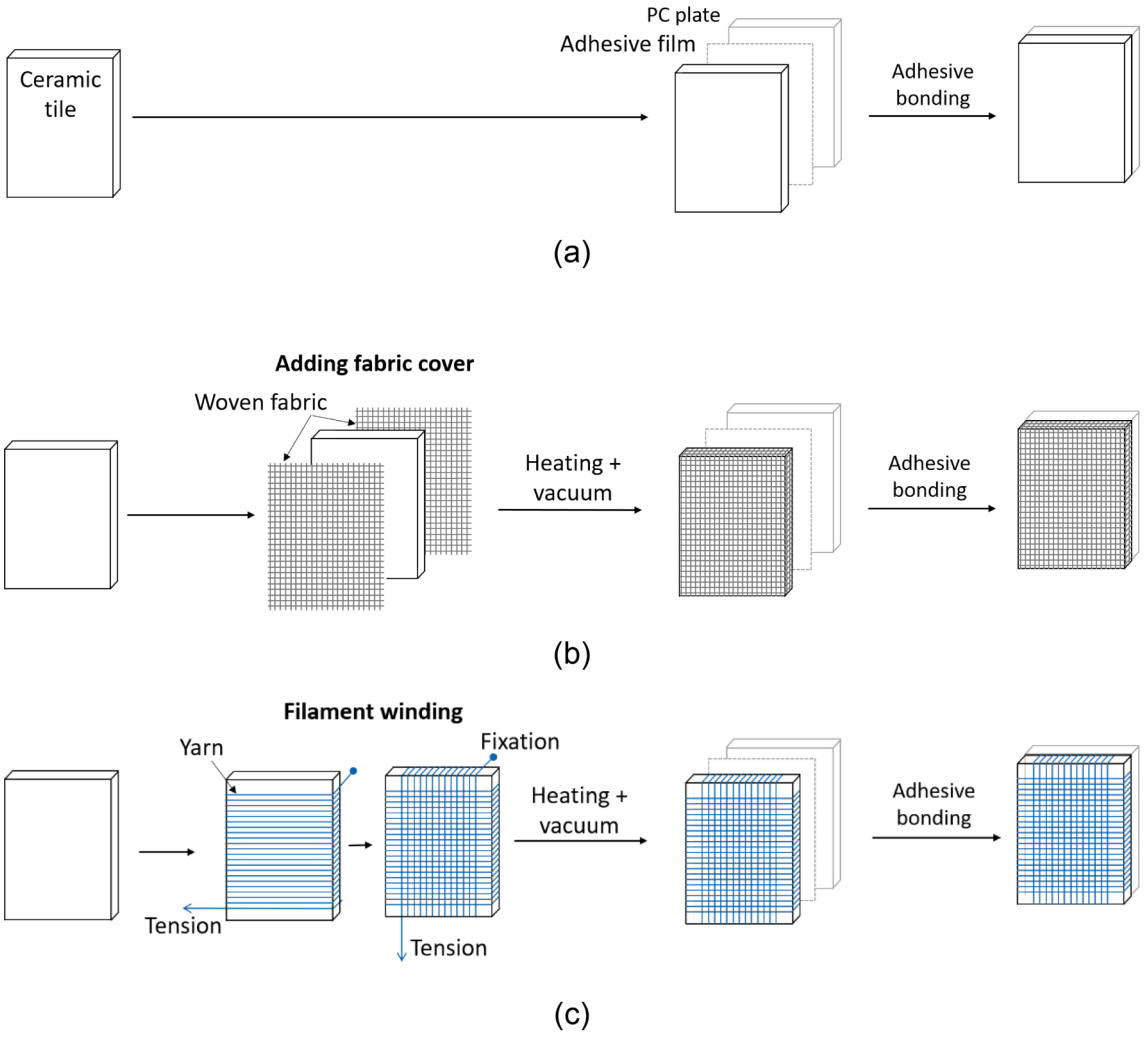

Fig. 1. Schematics showing the manufacturing of (a) the targets with the bare ceramic tile, referred to as Target A, (b) the targets where the woven fabric was wrapped around the ceramic tile, referred to as Target S (standard method), and (c) the targets where yarns were filament-wound around the ceramic tile in the 0° and 90° directions, referred to as Target N (new method).

covered by, or wrapped in, a sheet of high-tenacity fibre composite material [11–20]. When the ceramic is covered by a sheet material, the ceramic will be partly held together both during and after impact from the projectile. The fractured ceramic is then prevented from moving and is held in place in the path of the projectile. This gives more time for erosion and fragmentation of the core of the projectile. The sheet material will also contribute to improved multi-hit performance, since it introduces radial constraint on the ceramic surface. This prevents through-thickness cracks from opening and confines larger ceramic fragments that are formed during impact, hence improving the integrity of the tile after impact. Another effect of the sheet cover is to reduce the angle of spall that is ejected from the strike face.

Several studies have been conducted on the efficiency of different designs of hard armour plates, looking into factors such as the type of composite material, position of the composite cover (front and/or back of ceramic) and number of composite layers [20]. However, one topic that has received little attention is how pre-tensioning of composite materials or cladding layers affects the ballistic performance. One study by Jaitlee [21] investigated the effect of a composite cladding layer on the rear side of 4 mm silicon carbide tiles. In this work, the cladding was an aramid fabric that was pre-tensioned and then held in place by a cured epoxy. Ballistic testing was conducted with a 7.62 mm mild steel core projectile. No V_{50} data were presented, however, it was reported that pre-tension in the fabric produced a reduction in the back face signature. Although no explanation to this observation was given, the results seem to indicate an unexplored potential of pre-tensioning of composite sheets in hard armour plates.

Although not directly related to hard armour plates, some recent studies have investigated the effect of pre-tensioning of similar material systems. For example, Zhikharev et al. [22] investigated the ballistic impact response of a glass fibre-reinforced plastic (GFRP) laminate that was loaded in uniaxial tension during ballistic testing. It was observed that the V_{50} ballistic limit of a 6.35 mm diameter steel ball was decreased when the preload was increased. This observation was in part explained by less energy absorption in the preloaded composite. Tapie et al. [23] conducted impact experiments on woven high-strength fabrics that were pre-tensioned in the warp direction. Here, the V_{50} ballistic limit of a 12 mm diameter steel projectile was increased up to a critical level of pre-tension, after which the ballistic limit was reduced.

In this study, a unique method of applying the fibre-composite cover around the ceramic tile was investigated. The method consisted of filament winding of glass fibre yarns around the tile while simultaneously applying a pre-stress to the yarn. The filament winding was conducted in two directions around the tile, thus giving a composite sheet layer consisting of two plies with a 0°/90° lay-up on each side of the tile. Targets manufactured using this method were compared to

Table 1
Overview of the different types of targets.

Target description	Bare alumina	Standard method	New method
Target	A	S	N
Composite	n/a	Wrapped fabric	Filament-wound yarn
Alumina thickness (mm)	7.4	7.0	7.0
Areal density of alumina (kg/m^3)	28.5	27.0	27.0
Areal density of composite (kg/m^3)	n/a	$0.75 \times 2 = 1.5$	$0.375 \times 4 = 1.5$
Areal density PC of backing (kg/m^3)	9.6	9.6	9.6
Target areal density (kg/m^3)	38.1	38.1	38.1

targets that were manufactured using a standard method whereby a glass fibre fabric was wrapped around the ceramic. Targets that were made of bare alumina (no composite cover) were also included as reference. All three target types had a backing layer of polycarbonate (PC) and the same overall areal density of 38.1 kg/m^2.

Ballistic limit testing (V_{50}) was conducted to evaluate the ballistic performance of the targets. V_{50} is the velocity at which the probability of both perforation and stop is 50%. The targets were strapped to a metal frame and tested with a 7.62 mm AP projectile with a hard steel core. The residual projectile core fragments were collected and analysed.

2. Experimental

2.1. Target types, materials and manufacturing methods

Three different types of targets were manufactured by NFM Group AS (Ski, Norway), one reference target consisting of a bare alumina tile with a backing of polycarbonate, and two targets with a composite-covered alumina tile that was backed by PC. A schematic illustrating the different steps in the manufacture of the targets is shown in Fig. 1. The composite was placed around the alumina tile by two different methods. In the first target, a comingled glass fibre/thermoplastic polymer woven fabric was wrapped around the alumina, with one fabric layer on each side, see Fig. 1(b). This is a common method for manufacturing the ceramic component of hard armour plates and will be referred to as the 'standard method'. In the second target, yarns made of the same glass fibre/thermoplastic polymer were filament wound around the alumina. The filament winding was conducted by winding the yarn around the alumina in two directions, see Fig. 1(c), and as such producing a lay-up with a 0°/90° fibre orientation on each side of the tile. This manufacturing method will be referred to as the 'new method'. All targets were designed so that they had the same total areal density at the point of impact. Details about the different types of targets are given in Table 1.

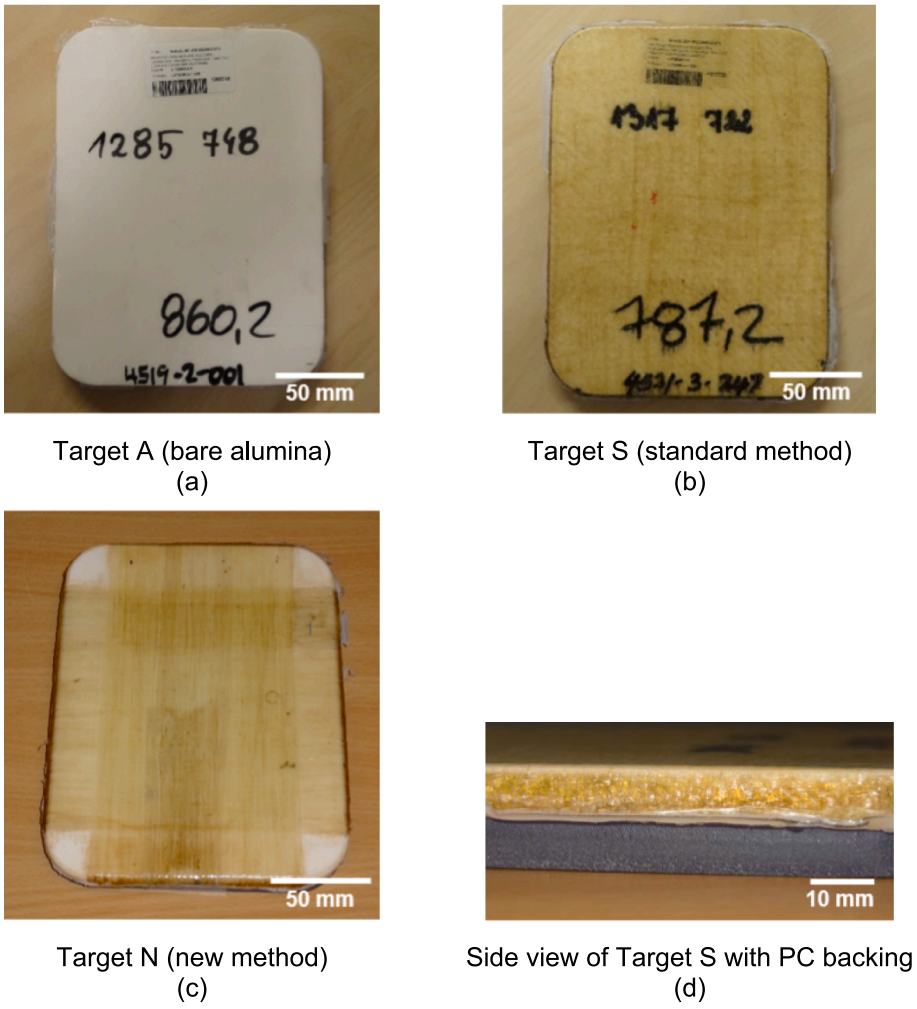

Fig. 2. Images of the different types of targets: (a) Target with bare alumina (Target A), (b) target produced by the standard method where the composite fabric was wrapped around the alumina (Target S), (c) target produced with the filament-wound yarn around the alumina (Target N), and (d) side view of Target S with PC backing.

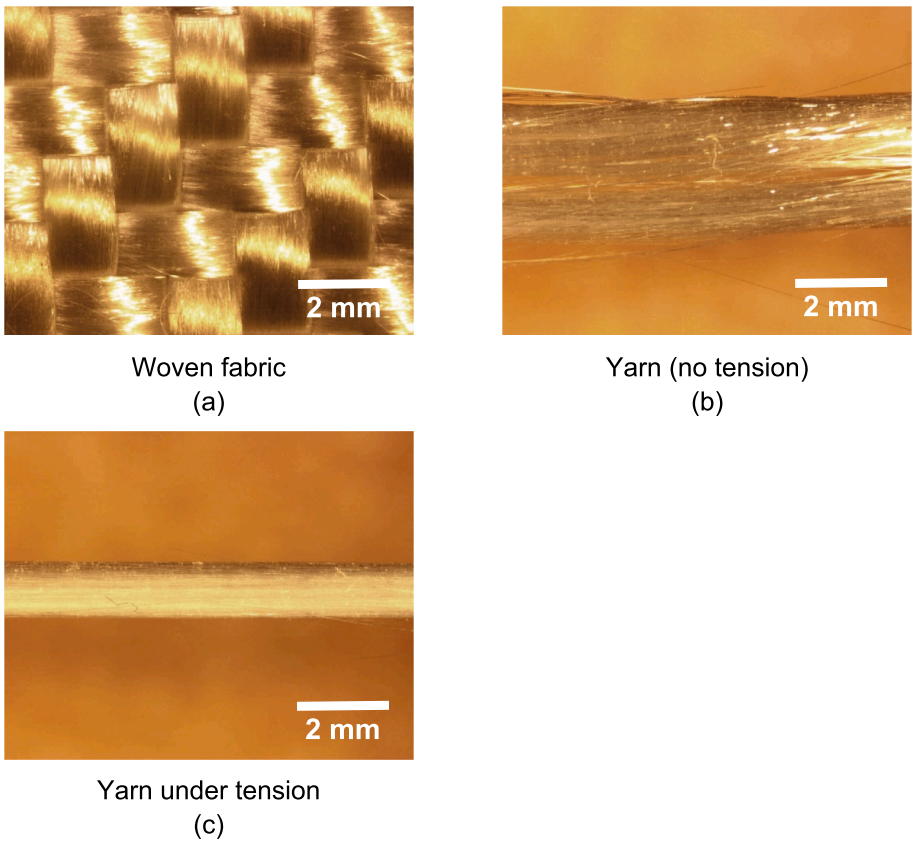

Fig. 3. Microscopy images of the (a) commingled glass/PET woven fabric, (b) the commingled glass/PET yarn, and (c) the yarn under tension.

The ceramic employed in the targets was 98% aluminium oxide (alumina, Al_2O_3) from Moh-9 Armour Ceramics (Pretoria, South Africa). The alumina ceramic tiles were all manufactured to measure 200 mm × 150 mm. Tiles of two different thicknesses were used; 7.4 mm and 7.0 mm, with areal densities of 28.5 kg/m^2 and 27.0 kg/m^2, respectively; see example in Fig. 2(a). The alumina that was employed in the two 'composite' targets had rounded edges to facilitate the application of the composite.

The fabric employed in the 'standard' targets (Target S) was a woven fabric (balanced twill 2/2) of comingled glass fibres and thermoplastic polyester (polyethylene terephthalate, PET) fibres delivered by Comfil (Gjern, Denmark), see Fig. 3(a). One layer of the fabric was wrapped around the ceramic tile. The alumina/composite target was then processed by a vacuum-assisted moulding process heated above 190 °C. This led to melting of the thermoplastic polymer, infiltration of the glass fibres and the formation of a consolidated matrix with low porosity content upon cooling, see Fig. 2(b). According to the material manufacturer, the nominal fibre content of the consolidated composite material was 57% by weight and 42% by volume, and the density was 1.87 g/cm^3. The thickness and areal density of one composite layer was 0.4 mm and 0.75 kg/m^2, respectively.

For the targets produced by the 'new method' (Target N), see Fig. 2 (c), a yarn consisting of the same glass fibres, the same PET fibres, and the same fibre content, with a linear density of 524 tex, was employed. The comingled yarn, as shown in Fig. 3(b-c), was delivered on rovings by Comfil. Filament winding of the yarn was conducted with a Pro's Pro Challenger I Stringer machine (RaquetDepot.co.uk, Emsworth, UK), keeping the yarn under tension during the application. As can be observed in Fig. 3(c), this results in a clearly defined, relatively circular shape of the yarn, as opposed to the un-tensioned yarn which has a more

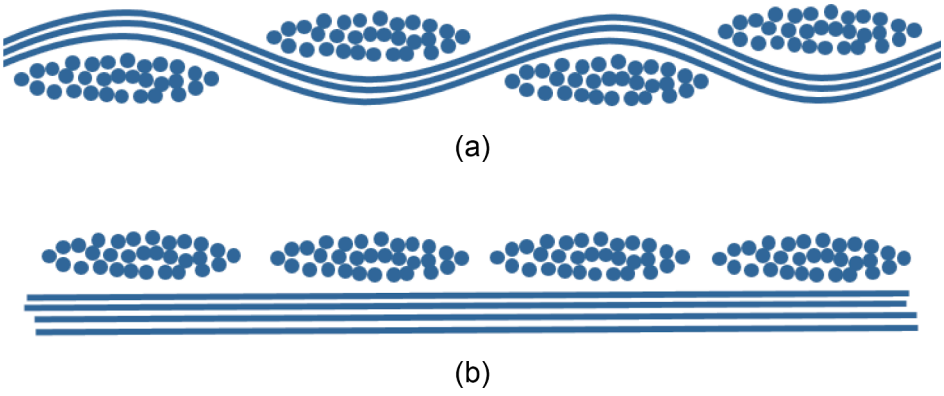

Fig. 4. Idealised schematics of the consolidated composite cross-sections: (a) One layer in a woven fabric (corresponding to Target S; standard method), and (b) one layer in a 0°/90° filament-wound composite (corresponding to Target N; new method).

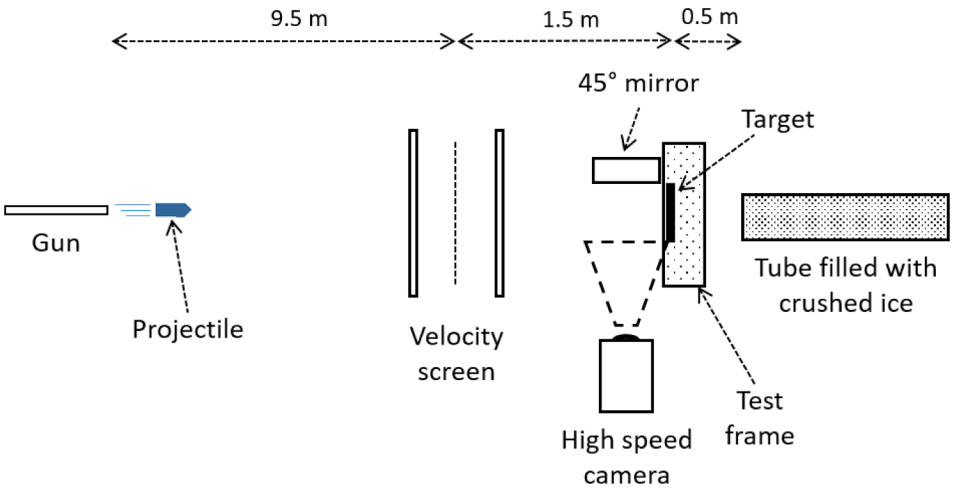

Fig. 5. Experimental setup for the ballistic testing.

'loose' structure, see Fig. 3(b). The yarns were placed side by side on the alumina under pre-tension, starting close to the edge of the tile, so that one composite layer was produced in each process cycle. The 0°/90° lay-up was created by repeating this process in the perpendicular direction on the alumina tile, see Fig. 1(c). No sign of fibre breakage was observed during the filament winding process. After melting and cooling, the characteristics of the composite were the same as for the fabric. However, the areal density of one layer in either the 0° or 90° direction is nominally 0.375 kg/m^2. The production method resulted in a target with a different lay-up and lower areal density close to the edges of the tile. However, the middle part with 'correct' lay-up was around 150 mm by 100 mm in size, see Fig. 2(c), so this is believed to have no influence on the ballistic tests results.

Idealised schematics of the cross-sections of the two different composite covers are shown in Fig. 4. The schematics illustrate that a certain degree of fibre waviness is to be expected in the consolidated composite made from the woven fabric, since the yarns are interlaced at right angles to each other, as shown in Fig. 3(a). In the filament-wound composite, on the other hand, the fibres will be more aligned in the 0° and 90° directions, having a fibre structure that is more similar to what is observed for the tensioned yarn in Fig. 3(c).

A flat and rectangular monolithic plate of transparent PC (Lexan, General Electrics) was used as backing material in all the targets, see Fig. 2(d). PC is a relatively common backing material, and provides support to the ceramic in a similar manner to that of UHMWPE or aramid backing systems [24]. The dimensions of the PC plate was 200 mm × 150 mm × 8 mm and the areal density was 9.6 kg/m^2. The PC backing was bonded to the ceramic or the composite, depending on the target type, see Fig. 1, in a second heating cycle above 130 °C using Pontacol BP22.2202 (Pontacol AG, Schmitten, Switzerland). Pontacol BP22.2202 is a double-sided adhesive film with a thermoplastic polyurethane on one side and a modified polyolefin on the other, thus allowing the adhesion of a range of dissimilar materials. The PU side was facing the PC backing, while the polyolefinic side faced the ceramic or the composite. The adhesive film had an areal density of 0.045 kg/m^2, which contributes little to the areal density of the targets.

In the initial part of the study, targets where the alumina was confined by an aramid yarn (Twaron 550 dtex f1000) around the outer perimeter were investigated. For each of the three target types, around half of the samples had the aramid confinement. However, analysis of the results showed that the edge confinement had no effect. The results for the unconfined and confined samples have therefore been merged to improve the statistical reliability for each of the three target types. Hence, the edge confinement will not be discussed further in this paper.

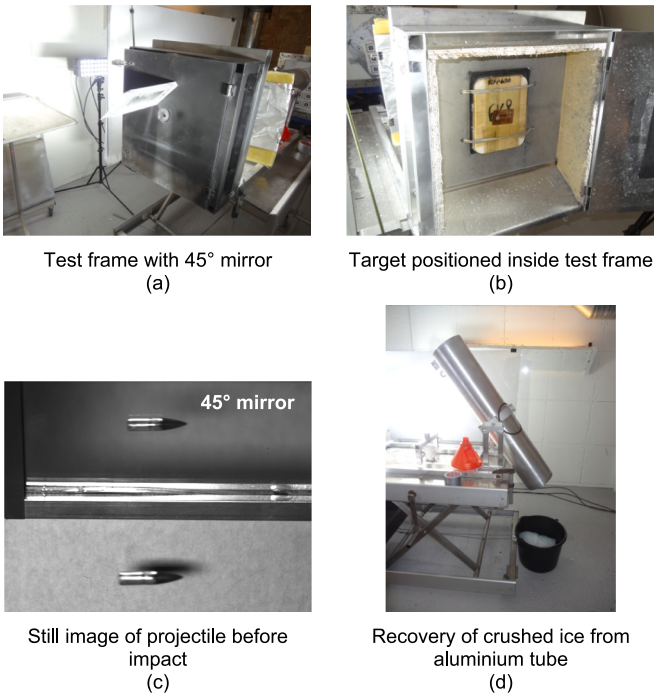

Fig. 6. Images from the ballistic testing: (a) Test frame for mounting of the target and recovery of non-perforating projectile fragments. A 45° angled mirror for yaw measurement of the projectile is attached to the front door. (b) Target positioned inside the test frame. The strike face of the target is facing outwards, with the front door of the test frame open. (c) Still image from a high speed video of the projectile prior to impact. The video of the projectile from two angles is used to calculate the combined yaw of the projectile. (d) Recovery of crushed ice inside the aluminium tube, which contains projectile fragments that have perforated the target.

2.2. Ballistic testing

The ballistic testing was conducted at the Norwegian Defence Research Establishment (FFI; Kjeller, Norway) using the experimental test set-up illustrated in Fig. 5. During the testing, the targets were placed in a custom-made aluminium frame, see Fig. 6(a), and shot with no additional backing. The test frame consisted of an aluminium box that surrounded the targets, with doors at the front and rear. In addition, there were holes for the projectile and the fragments to pass through. This box was used to minimize scattering of debris from the testing, and

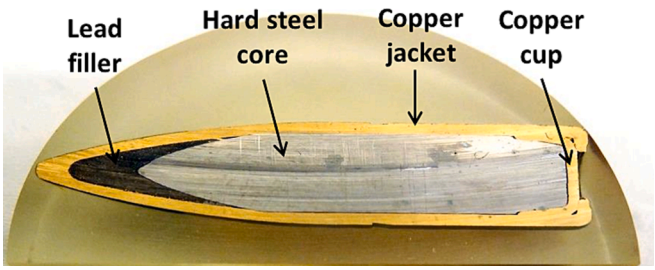

Fig. 7. Cross-section of the 7.62 × 63 mm M2 AP projectile used for the ballistic testing [20].

to more easily recover the remains of the targets and the projectiles after testing. The targets were held in place in the frame with elastic bands, see Fig. 6(b). All targets were shot only once and then discarded. Around 55–60 targets of each type were tested, resulting in around 50 valid tests of each type.

The projectile used for testing was 7.62 × 63 mm M2 AP, shown in Fig. 7. This projectile has a 5.19 g AP hardened steel core, a 0.7 g lead filler in front of the steel core, a 0.4 g copper cup and a 4.4 g copper jacket [25]. The total mass of the projectiles used for the tests was on average 10.56 ± 0.01 g (±standard deviation). A powder gun with a test barrel (Prototypa, 1:12 twist, 562 mm bore length) was used to accelerate the projectile. The powder used was N540 from Vihtavuori (Vihtavuori, Finland), except for impact velocities < 460 m/s where powder N32C was used. A light velocity screen (LS-04, Prototypa, Brno, Czech Republic), located 9.5 m from the from the gun barrel, was used to measure the projectile velocity with the target strike face positioned at a distance of 11.0 m. The impact velocity at the target position was corrected for the effect of drag between the velocity screen and the target, and a correction factor of 0.73 m/s/m was employed [26].

Projectile yaw was observed by a mirror placed in front of the point of impact, as shown in Fig. 6(a). The mirror was angled at 45° so that the projectile could be filmed from two directions by a high-speed camera (Photron FASTCAM Mini AX200 type 900 K, Photron Europe Limited, West Wycombe, UK) at 20 000 fps and at a distance of 5 to 25 cm in front of the target, see Fig. 6(c). The shot was considered not valid if the

Target A, PP, 582 m/s. Front view of ceramic tile.
(a)

Target A, PP, 582 m/s. Back side of the PC plate.
(b)

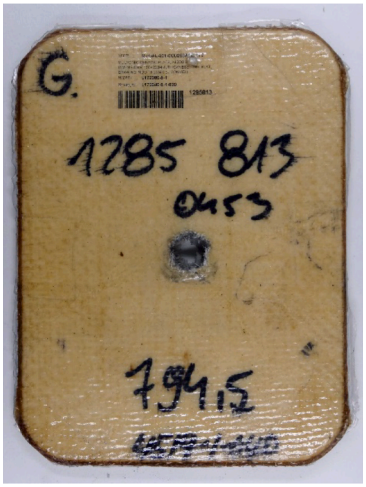

Target S, CP, 640 m/s. Front view of ceramic tile with fabric cover.
(c)

Target S, CP, 640 m/s. Back side of ceramic tile with fabric cover.
(d)

Fig. 8. Images of tested targets after non-perforating and perforating shots: (a-b) Bare alumina, including PC backing, (c-d) Target S (standard method), and (e-f) Target N (new method). The impact velocities are within the zone of mixed results for that particular type of target.

Target N, CP, 637 m/s. Front view of ceramic tile with filament-wound cover. (e)

Target N, CP, 637 m/s. Back side of ceramic tile with filament-wound cover. (f)

Fig. 8. (*continued*).

combined yaw exceeded more than 10°. In several ballistic test standards, a maximum yaw of 5° is permitted [27,28]. However, at the lower velocities it was difficult to shoot consistently within this lower yaw limit. With this in mind and analysis of results indicating that choosing either 5° or 10° as yaw limit did not significantly influence on the results, a yaw limit of 10° was chosen (see Appendix A). The point of impact was always within 10 mm of the centre of the targets. With the relatively large target size that was employed here, the point of impact had negligible influence on the results.

The targets were tested over a wide range of impact velocities with initial tests performed as close as possible to 10 predetermined impact velocities in the range from 400 m/s to 800 m/s (400 m/s, 450 m/s, 500 m/s, 550 m/s, 575 m/s, 600 m/s, 650 m/s, 700 m/s, 750 m/s and 800 m/s) for each of Targets A, S and N. The desired impact velocity for the following 10 shots for each target type was determined using the up/down method [29] with increments in velocity of 15 m/s per shot, beginning from the first estimated V_{50} value. The final shots were placed at velocities around the preliminary V_{50} value, estimated from all the previous shots and up to 100 m/s higher velocities. The aim of these shots was to obtain more information about the core fragmentation at velocities just above the perforation threshold. Invalid shots with excessive yaw (above 10°) were excluded from the data sets after all testing was concluded. Valid shots in the range from 376 to 802 m/s were obtained. It should be noted that the targets with and without the aramid thread around the edge were tested separately using this approach, after which the results were merged.

Complete penetration (CP) (or perforation) [26] was assessed by a double layer of 0.05 mm aluminium foil that was placed behind the target. The perforating residual projectiles were collected using a bag of crushed ice that was placed inside a hollow aluminium pipe to absorb the residual energy and stop the fragments. The pipe was designed so that it could be tilted after the test, and the crushed ice containing the fragments was poured into a bucket, see Fig. 6(d). The ice was then melted and the fragments recovered. In the case of partial penetration (PP) (or non-perforation) taking place, the projectile fragments were located inside the custom-made box. In both cases, the mass of the largest residual core fragment of the projectile was measured. In a small number of the tests the core fragments were not captured by the pipe or the box.

The V_{50} ballistic limit velocity was determined using the probit regression model with the maximum likelihood method. The probit model can be used for binary data, as is the case for ballistic impact, with two outcomes; either partial perforation (PP) or complete perforation (CP). By choosing the probit model it is assumed that the probability of perforation as function of impact velocity has a shape that can be approximated by the probability density function (PDF) of the normal distribution [26,30]:

$$PDF = \frac{1}{s \bullet \sqrt{2\pi}} e^{\frac{-(V-V_{50})^2}{2 \bullet s^2}}, \quad (1)$$

where V_{50} is the mean value of the normal distribution, s is the standard deviation of the normal distribution and V is the impact velocity. The probit model also allowed for the calculation of the 90% confidence intervals (CI).

3. Results

3.1. Targets after testing

Pictures of some targets after ballistic testing are shown in Fig. 8. These examples are from targets that were tested at velocities within the zone of mixed results, i.e. in the velocity range where overlapping PP and CP shots are observed. One common observation for all targets was that the PC plate often detached from the composite or ceramic, depending on the target type, during the testing. An example of a detached PC plate, from a test resulting in partial perforation of Target A, is shown in Fig. 8(b). Dishing of this PC plate took place at the point of impact and a small bump was formed at the back side. This was a common observation for PP shots, however, significant 'petalling' of the PC was observed for CP shots, which was probably preceded by some dishing [31]. It was observed for only a few targets that the PC plate was fragmented into a few larger pieces.

Fig. 8(a) shows the largest ceramic fragments from a 582 m/s impact on Target A (bare alumina) resulting in a partial perforation. The tile fragments are placed with the strike face up and radial cracks from the point of impact are clearly seen. As the picture illustrates, the alumina ceramic was heavily fractured during the impact process, with the fragments formed at the point of impact, and inside the region where cone cracks are formed, generally being much smaller. All targets of type A exhibited this type of failure.

For both target types with a composite cover, Targets S and N, the damage to the ceramic tile was not easily observed with the naked eye as the glass fibre composite was not heavily damaged and the fragments were held better in place. Fig. 8(c-d) shows an example of an impact at

Fig. 9. Close-up of strike face and point of impact showing typical composite failure: (a) Little composite failure outside the point of impact in Target S (standard method). (b) Fibre delamination from the point of impact and towards the edge in Target N (new method).

640 m/s on Target S (standard method) resulting in a perforation. There is a hole in the ceramic at the point of impact, but the damage to the ceramic tile is not easily observed due to the presence of the composite cover. However, on the back side of the ceramic, the size of the cone area is visible as a darker region where the composite has detached from the ceramic. Despite the definitive presence of radial cracks, these are not easily observed. For Target N (new method), an example of a perforating impact at 637 m/s is shown in Fig. 8(e-f). Similar damage is observed for this target, with a few radial cracks visible in the uncovered upper left corner. The ceramic is heavily fragmented, something that can be observed under good lighting conditions. Remnants of the film adhesive can also be seen on the back side of the composite.

Typical composite failures at the point of impact are shown in Fig. 9. Similar failure was also observed at the back side of the ceramic. Very little composite damage was observed outside the actual point of impact in the fabric-wrapped targets (except the ceramic/composite delamination described above). For the filament-wound targets, however, significant delamination in the outermost layer is observed in the longitudinal fibre direction, see Fig. 9(b). Here, the fibre failure is extending from the point of impact towards the edge of the target.

3.2. Ballistic limit velocity

The results from the ballistic testing of the three different targets are presented in Fig. 10, where all the valid non-perforating and perforating shots are plotted. The probability of perforation, as determined by the probit method, is indicated together with the 90% confidence limits. A probability of perforation of 0.5 corresponds to the V_{50} ballistic limit value for a particular target. The values of the V_{50} and the 90% confidence intervals are shown in Table 2. The three different types of targets gave very different values of V_{50}.

The target with the bare alumina tile (Target A) had a V_{50} of 586 m/s. This target had the same areal density, but a slightly thicker alumina tile than the two alumina/composite targets, 7.4 mm and 7.0 mm, respectively. The target where the composite fabric was wrapped around the alumina tile using the standard production method (Target S), had a V_{50} of 536 m/s. The difference in V_{50} between Targets A and S can be distinguished by the different thickness of the alumina in the targets.

Interestingly, Target N with the composite yarn wound around the tile, had a high V_{50} value of 622 m/s. This is as much as 16% higher than the V_{50} of the standard target where the fabric was wrapped around the tile, even though the ceramic thickness and the target areal densities were the same for the two targets. The only difference was the method in application of the composite around the tile and the different lay-up of the composites. It is also noteworthy that Target N gave a higher V_{50} than the bare alumina target. The difference was statistically significant with the 90% confidence limits that were employed, see Table 2.

3.3. Fragmentation of the projectile core

All the ballistic tests resulted in erosion and fragmentation of the steel core of the 7.62 × 63 mm M2 AP projectile, both for PP and CP shots. Here, we chose to only consider the residual mass, m_{res}, of the largest core fragment in the discussion of the core fragmentation. The main reason for this is that the largest fragment most likely has the highest kinetic energy, and therefore the highest probability of perforation of an armour system. Having said this, it is important to highlight that a 'fragment cloud' of several smaller fragments might pose a more serious threat; an issue that is not considered here. It is similarly important to remember that this areal density of alumina armour would be worn in conjunction with soft armour, and normally backed with UHMWPE or aramid.

Examples of residual core fragments are shown in Fig. 11, with two examples presented for each type of target; one fragment from a PP shot and one from a CP shot. All fragments shown are from the tail of the hard steel core. The largest fragment in all tests performed in this study, both for PP and CP shots, were from the tail. It is clear from the six core fragments presented here, that the damage mechanisms for the hard steel core when striking the hard alumina ceramic is not deformation, but fragmentation due to erosion and crack formation, then mainly of the tip of the core. This has been discussed in more detail in other studies [20] and will therefore not be discussed any further in this paper.

The mass of the largest residual core fragment for all the tests is shown in Fig. 12. The diagram shows a great deal of scatter in the data. Moreover, it highlights the ability of different shots at similar impact velocities to give different residual core masses. This is as expected, since the ballistic impact is a stochastic event, giving different fragment masses after impact on identical targets [20].

As can be seen in Fig. 12, a high number of results over a large velocity span give rise to very different core erosion and fragmentation, and the results can be difficult to compare. The average masses for PP and CP shots were therefore compared for three velocity regions, 500–575 m/s, 575–650 m/s and 650–725 m/s. The velocity region of 500–725 m/s very roughly overlaps with the V_{50} and V_{50} + 100 m/s for the three types of targets. The results are summarised in Table 3, together with the 95% confidence levels of the average masses and the number of valid tests in each case.

For PP shots at lower impact velocities, 500–575 m/s, the results in Table 3 show that the average mass of the largest projectile fragment is lowest for Target A (2.9 ± 0.5 g), which has a slightly thicker ceramic

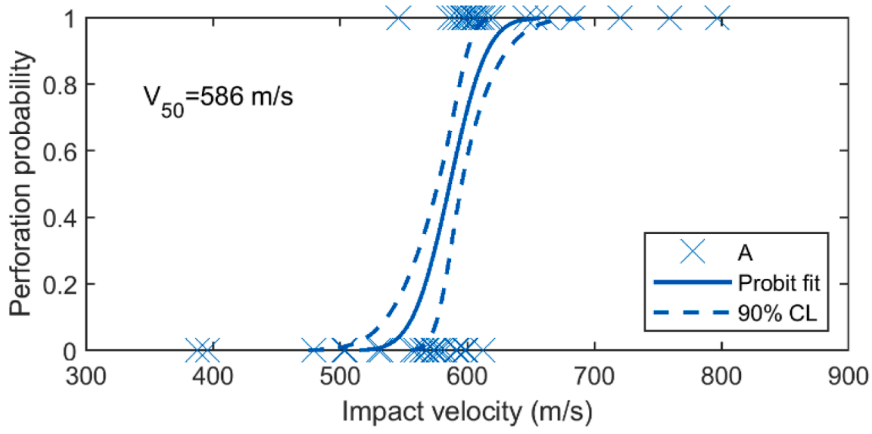

(a)

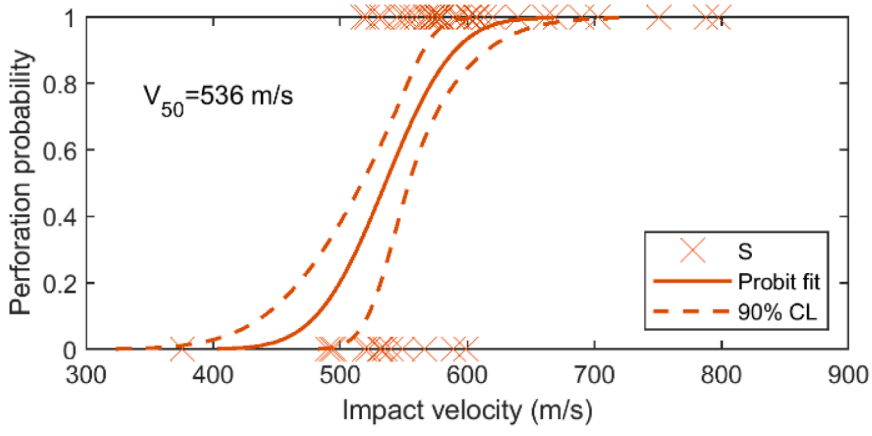

(b)

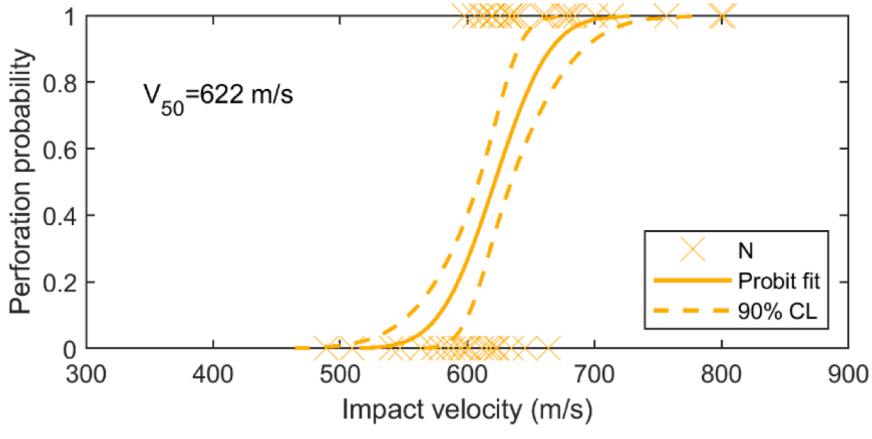

(c)

Fig. 10. Probability of perforation for (a) Target A (bare alumina), (b) Target S (standard method), and (c) Target N (new method).

Table 2
Ballistic limit velocity with 90% confidence intervals (CI) for the different types of targets.

Target	V_{50} (m/s)	90% CI at V_{50} (m/s)
A (bare alumina)	586	[577–596]
S (standard method)	536	[517–554]
N (new method)	622	[609–634]

than Targets S and N. The mass for Targets S and N is the same (3.5 ± 0.5 g and 3.5 ± 0.7 g, respectively), which suggests that the fragmentation of the steel core is primarily linked to ceramic thickness when no perforation is taking place within this velocity range. For Target S, CP shots gave a higher fragment mass than PP shots. This is not surprising since a more eroded and fragmented steel core is more likely to be stopped compared to a more intact core. It is notable that within this velocity range there were no valid CP shots for Target N, as opposed to

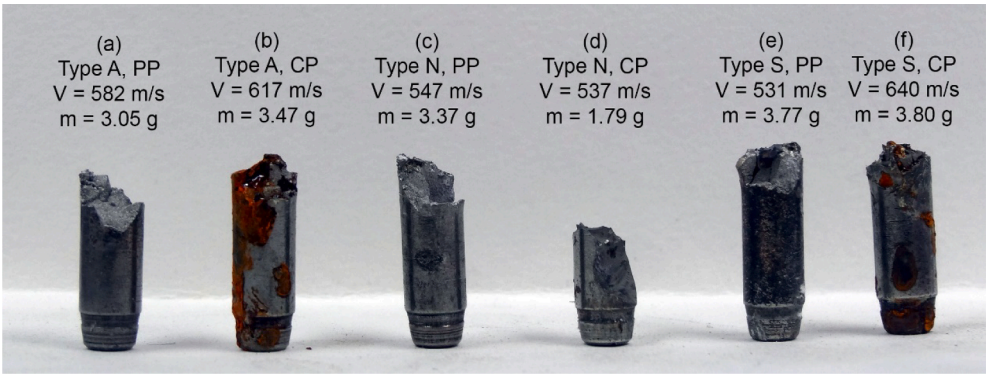

Fig. 11. Examples of core fragments from non-perforating (PP) and perforating shots (CP): (a-b) Bare alumina, (c-d) Target N (new method), and (e-f) Target S (standard method). The impact velocities and the residual fragment masses, m_{res}, are presented in the image.

12 for Target S. (Most shots on Target N were conducted at higher velocities.).

In the velocity range from 575 m/s to 650 m/s, the average fragment mass is reduced compared to the lower velocity range. The PP shots for all types of targets exhibit the same degree of core fragmentation (although there are very few data points for Target S). However, for the CP shots in this velocity range the difference in fragment mass is obvious. The fragment mass of Target N is 2.5 ± 0.5 g, while the masses of Targets A and S are 3.3 ± 0.5 g and 3.4 ± 0.4 g, respectively. These results are statistically solid with 13, 17 and 14 valid tests included in the average values. Most notably, this suggests that not only does Target N have a significantly higher V_{50} than Target S, but the core erosion/fragmentation for perforating shots in this velocity range (which is around the V_{50} for Target N) is also much higher for targets made of the same composite/alumina materials and with the same areal density. The combination of a higher V_{50} and more core fragmentation of perforating shots, will result in a much lower residual kinetic energy of the perforating core fragments for Target N. The effect is the same, although not as pronounced, when comparing target N to target A with the thicker ceramic.

In the velocity range from 650 m/s to 725 m/s there was a lower number of valid shots. Nevertheless, the average mass of CP shots for Target N was much lower compared to Target S also at these higher velocities, again indicating a higher performance of the new target design.

A more visual way of presenting the data on the core fragment masses is shown in Fig. 13, where the data points represent average masses that were calculated from more narrow velocity ranges than those used in Table 3. In the table, a velocity range of 37.5 m/s was used. Data from all valid shots at all velocities are included in the figure. The observed trends are the same in Fig. 13 and Table 3, however, Fig. 13 gives some additional insight into the fragmentation behaviour of the projectile.

When comparing the PP shots for all three types of targets, there seems to be a tendency towards smaller residual fragment mass with increasing impact velocity, independent of target type. The lighter fragments are likely the result of more core erosion and fragmentation which is taking place at the higher impact energy densities at the higher velocities. As expected, higher velocity gives lower residual mass. Increased erosion of the tip of a 7.62 mm hard steel core projectile with increasing impact velocity has previously been observed [14], although at lower velocities than those employed here. However, a similar relationship between impact velocity and residual fragment mass is not observed for the CP shots.

One striking observation in Fig. 13, similar to that discussed above in relation to the data in Table 3, is the significant difference in fragment mass for CP shots of the two composite-covered alumina targets, Targets S and N. For Target S, the V_{50} is 536 m/s and the fragment mass above this velocity is ~ 3.7 g. The mass appears to remain relatively constant even at higher velocities up to around 720 m/s. For Target N, the V_{50} is 622 m/s and the fragment mass is much lower at ~ 2.5 g. This difference in mass between the two targets exists even at similar impact velocities. Hence, it seems clear that Target N produced by filament winding of the composite gives higher core fragmentation of the perforating bullets. Depending on exactly what residual masses are compared, Target N gives a reduced fragment mass by 25–35% compared to Target S. For Target A with the bare alumina of slightly higher thickness and a V_{50} of 586 m/s, the residual mass for CP just above the V_{50} was ~ 3.4 g, which is similar to that of Target S and much higher than Target N.

For increasing impact velocities, the residual mass for CP shots for Target S gets closer to that of Target N. At impact velocities above ~ 740 m/s, there seems to be a region where the residual fragment mass of all the different targets are grouped together at ~ 3 g. This was particularly true for the two composite/alumina targets, however, whether this is a real effect or just a coincidence is unclear.

4. Discussion

The results clearly showed that the production method where the fibre material was filament-wound around the ceramic (Target N), with a pre-tension in the glass fibre yarn, gave improved ballistic performance compared to the method where the ceramic was wrapped in a fabric (Target S). Despite having the same alumina thickness and the same areal density, the filament-wound target gave a significantly higher V_{50} and significantly more fragmentation of the projectile steel core after perforation. The target also exhibited better performance compared to the bare alumina target with the higher ceramic thickness (Target A).

The most likely explanation for the increased performance of Target N, is related to the orientation of the fibres in the composite and, to some extent, the fibre pre-tension. In the filament-wound composite, the fibres are present in a lay-up with two individual 0°/90° plies. Each ply consists of unidirectional, highly aligned glass fibres. The fibres in the fabric, on the other hand, are woven and therefore have a certain degree of waviness, i.e. the glass fibres are not as straight as in the unidirectional plies, as illustrated in Fig. 4. It is well known that fibre waviness may reduce the mechanical properties of fibre-reinforced composites [32], and it has also been shown that even fibre waviness within a yarn can give reduced tensile strength [33]. The fibre orientation may be of importance during ballistic impact, where ceramic cracking is initiated as a result of tensile forces that are acting on the back side of the ceramic. A composite cover may act as a support and contribute to a delay in the opening of tensile cracks. In the fabric material, stretching of the fibres will have to take place, at least to some extent, before they are 'activated' and able to take up load. However, in the unidirectional plies the fibres are already highly aligned and able to take up load more quickly.

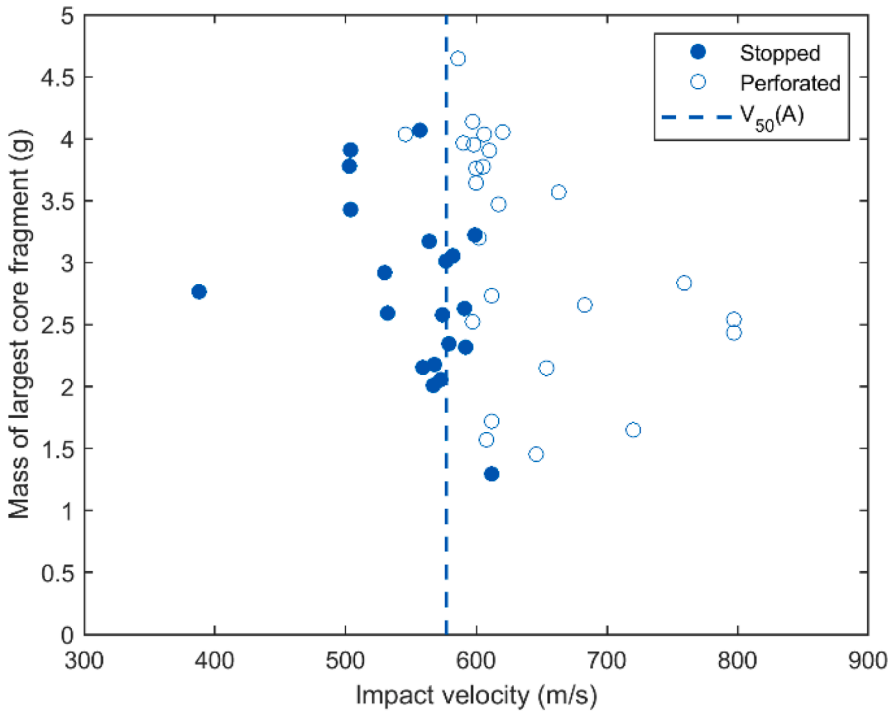

Target A
(a)

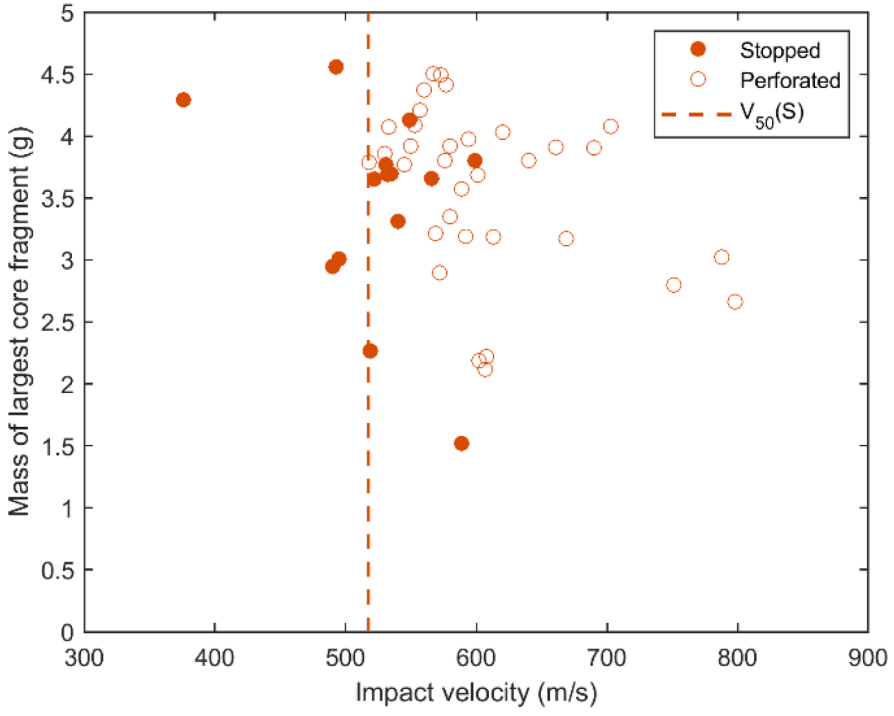

Target S
(b)

Fig. 12. The mass of the largest residual core fragment vs impact velocity for (a) Target A (bare alumina), (b) Target S (standard method), and (c) Target N (new method), for both non-perforating (PP) and perforating (CP) shots.

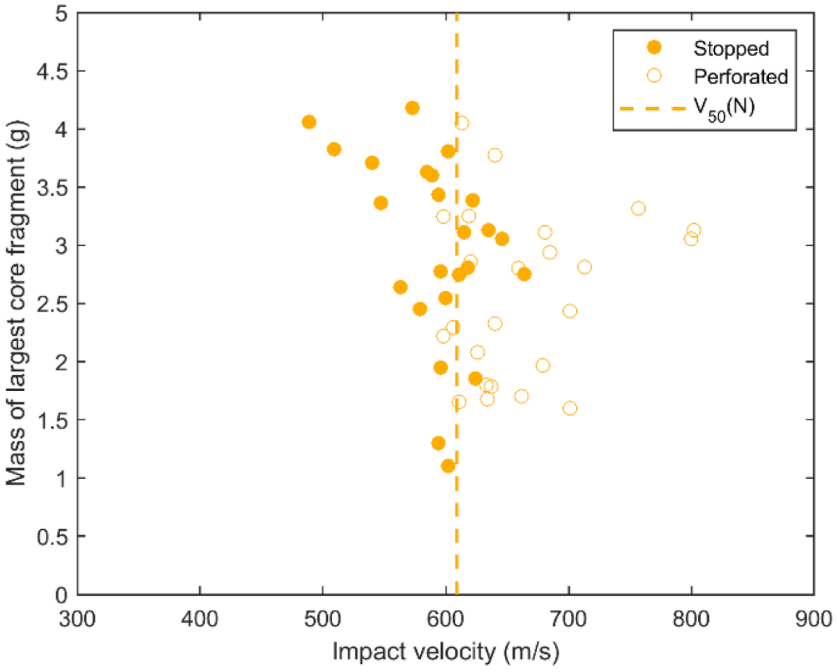

Target N
(c)

Fig. 12. (*continued*).

Table 3
Mass of largest residual core fragment in three velocity ranges for non-perforating (PP) and perforating (CP) shots. Average masses with 95% confidence intervals are presented together with the number of valid PP/CP shots for each target.

	PP		CP	
Impact velocity and target type	**Number of valid results in range**	**Avg. mass of largest core fragment ± 95% CI (g)**	**Number of valid results in range**	**Avg. mass of largest core fragment ± 95% CI (g)**
500–575 m/s				
A	12	2.9 ± 0.5	1	4.0 ± n/a
S	8	3.5 ± 0.5	12	3.9 ± 0.3
N	5	3.5 ± 0.7		
575–650 m/s				
A	7	2.6 ± 0.6	17	3.3 ± 0.5
S	2	2.7 ± 14.5	14	3.4 ± 0.4
N	17	2.7 ± 0.4	13	2.5 ± 0.5
650–725 m/s				
A			4	2.5 ± 1.3
S			4	3.8 ± 0.6
N	1	2.8 ± n/a	8	2.4 ± 0.5

Number of valid shots in the 500–725 m/s velocity range: A = 41, S = 40, N = 44.

This may result in the effect observed in Fig. 9(b), where the filament-wound composite has failed in the longitudinal fibre direction from the point of impact outwards. No such effect was observed for the fabric-wrapped composite. The pre-stress in the fibres may be of additional benefit since the fibres have already partly been strained during the manufacturing process. Zhikharev et al. [22] observed that the energy absorption and the V_{50} of GFRP laminates were decreased with increasing preload. This suggests that the fibres have been strained to be closer to the failure limit, which is negative for the capability of absorbing projectile energy in laminates. However, in the present study, the composite is acting as a support on the back side of a ceramic and such an effect may be positive for the overall target performance since the composite is able to delay the opening of tensile cracks more efficiently. If this hypothesis is true, then the composite cover on the back side is much more important than the cover on the front side.

Other mechanisms than those discussed above might potentially have some influence on the measured ballistic performance. For one, there is evidence in the literature that providing some lateral pre-stress to the ceramic is beneficial to ballistic performance [34–36]. The lateral pre-stress is usually applied by shrink fitting of a metal confinement around the ceramic tile. The investigated materials and the level of induced pre-stress varies between different studies, but positive effects have been observed for alumina tiles of similar thickness to those employed in the present study. Another potential effect is related to dynamic preloading of the ceramic during impact from projectiles with a lead filler, such as the 7.62 × 63 mm M2 AP projectile that was employed in the present study, see Fig. 7. For this type of projectiles, Elgy et al. [37] observed that the presence of a thin sheet cover material on the ceramic had a positive effect. The suggested mechanism behind this improvement was that the sheet cover allows the lead filler to spread on the surface of the target before the core engages with the ceramic. This spreads the area of interaction for the lead filler (and the jacket) over a larger area prior to the impact of the core, which gives less severe loading of the ceramic. It was also suggested that a confining pressure on the ceramic might further enhance the performance. These effects may be more pronounced for the presumably stiffer, filament-wound cover. Nevertheless, from the investigations in the present study, it is unclear if any of these effects contribute to the measured performance.

As mentioned before, there is a lot of scatter in the some of the data and therefore not too many conclusions should be drawn from these tests. Having said this, around 50 valid shots on each target type were

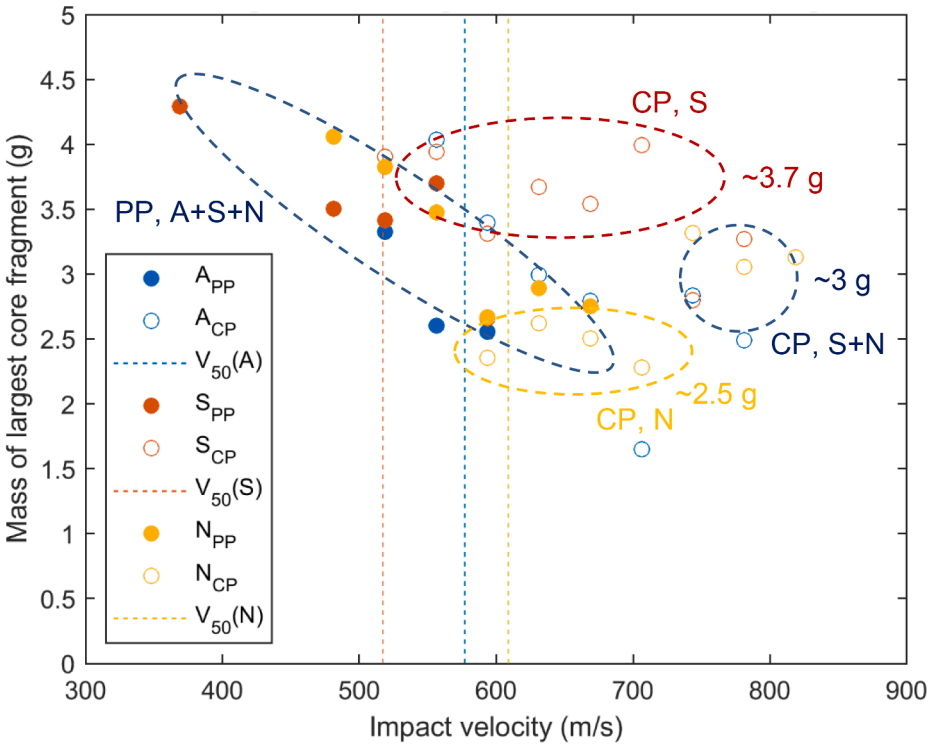

Fig. 13. Residual core fragment masses for both non-perforating (PP) and perforating (CP) shots. One point represents the average mass calculated from the individual results in a 37.5 m/s velocity range. The ellipses indicate approximately in what region the results for either PP or CP shots of different target types are located in the graph.

obtained (approximately 25 PP and 25 CP shots). It is therefore believed that some assumptions can be made with a certain degree of reliability. Overall, these results show some possible effects that, although so far unexploited and not yet fully understood, may represent a potential new path in the development of body armour systems. The observed effects from pre-tensioned fibres in composite covers on ceramics have, to our knowledge, not been reported elsewhere.

5. Conclusions

A novel production method for hard armour plates was investigated. The production method involved filament winding of pre-tensioned yarns of glass fibres around an alumina tile, resulting in a 0°/90° lay-up with highly aligned fibres. The new production method was compared to a standard method, in which a glass fibre fabric was wrapped around the alumina. Both types of glass fibre materials were comingled with PET fibres that melted and consolidated when heat-processed. A reference target consisting of bare alumina of slightly higher thickness was also prepared. All targets had a backing of PC and the same overall areal density at the point of impact.

Ballistic testing was conducted with a 7.62 mm AP projectile with a hardened steel core. Some very interesting observations were made:

- The filament-wound target had a much higher V_{50} ballistic limit value than the fabric-wrapped target, by as much as 16%. This was, despite having the same alumina thickness and areal density, producing a statistically significant difference in V_{50}. The only difference between the two targets was the different lay-up of the glass fibres in the composite cover.
- The fragmentation of the projectile steel core was much higher for perforating shots on the filament-wound target, compared to shots on the fabric-wrapped target. There was a significant difference in the residual mass of the largest fragment also at similar impact velocities.
- The filament-wound target gave higher V_{50} and higher core fragmentation than the bare alumina target, despite the higher alumina thickness in the bare target (and identical target areal densities).

A possible mechanism for the observations was discussed. The filament-wound composite has two individual 0°/90° plies of unidirectional, highly aligned glass fibres, and the fibres are also pre-stressed during target manufacture. This in contrast to the fabric-wrapping, where the fibres are woven and have some waviness. The high degree of fibre orientation may result in the fibres being 'activated' earlier in the impact process, providing better support for the ceramic. Hence, this may contribute to a delay in the opening of tensile cracks on the back side of the ceramic, giving more time for the projectile to interact with the target. Other mechanisms, such as dynamic preloading of the ceramic surface, might also contribute.

CRediT authorship contribution statement

Dennis B. Rahbek: Methodology, Formal analysis, Investigation, Writing – review & editing, Visualization. **Gwyn E. Roberson:** Conceptualization, Methodology, Writing – review & editing. **Bernt B. Johnsen:** Methodology, Investigation, Writing – original draft, Writing – review & editing, Visualization.

Declaration of Competing Interest

The authors declare that they have no known competing financial interests or personal relationships that could have appeared to influence the work reported in this paper.

Data availability

The test data have been shared as a supplementary file.

Table A1
Calculated results where all valid shots with yaw angles up to 5° or 10° have been included in the analysis of the ballistic limit velocity.

Target	5° yaw limit		10° yaw limit	
	V_{50} (m/s)	90% CI at V_{50} (m/s)	V_{50} (m/s)	90% CI at V_{50} (m/s)
A (bare alumina)	588	[572–603]	586	[577–596]
S (standard method)	516	[482–550]	536	[517–554]
N (new method)	630	[613–646]	622	[609–634]

Acknowledgements

The authors would like to acknowledge Marcin Lewicki (NFM) for assistance with sample manufacture, and Lasse Sundem-Eriksen and Ole Andreas Haugland (FFI) for conducting the ballistic testing. The main part of this work was carried out as part of the European Defence Agency-project CERAMBALL, contract number B 1091 GEM1 GP.

Appendix A

Ballistic impacts with a maximum yaw of 10° was included in the analysis of the ballistic limit velocity, although several ballistic test standards state a yaw limit of 5°. In these tests, the inclusion of shots based on a yaw limit of 5° or 10° had little influence on the calculated ballistic limit velocity, see Table A.1, and a yaw limit of 10° was allowed to include more data in the analysis, hence improving the statistics. One minor difference is observed for the targets produced by the standard method (Target S), where the V_{50} is 20 m/s lower when only the shots with a maximum yaw of 5° is considered.

Appendix B. Supplementary material

Supplementary data to this article can be found online at https://doi.org/10.1016/j.compstruct.2023.117452.

References

[1] Crouch IG. Introduction to armour materials. In: Crouch IG, editor. The Science of Armour Materials, ch. 1. London: Woodhead Publishing; 2017. p. 1–54.
[2] Hazell PJ. CERAMIC ARMOUR: Design and Defeat Mechanisms. Canberra, Australia: Argos Press; 2006.
[3] Lewis E, Carr DJ. Personal Armour. In: Bhatnagar A, editor. Lightweight Ballistic Composites: Military and Law-Enforcement Applications. Second Edition ed. Cambridge, United Kingdom: Woodhead Publishing; 2016. p. 217–29. ch. 7,.
[4] Crouch IG. Body armour - New materials, new systems. Defence Technology 2019;15(3):241–53.
[5] Wilkins ML, Cline CF, Honodel CA. Fourth Progress Report of Light Armor Program. Livermore, California, USA: UCRL-50694; 1969.
[6] Shockey DA, Marchand AH, Skaggs SR, Cort GE, Burkett MW, Parker R. Failure phenomenology of confined ceramic targets and impacting rods. Int J Impact Eng 1990;9(3):263–75.
[7] Sherman D, Ben-Shushan T. Quasi-static impact damage in confined ceramic tiles. Int J Impact Eng 1998;21(4):245–65.
[8] Shockey DA, Simons JW, Curran DR. The Damage Mechanism Route to Better Armor Materials. Int J Appl Ceram Technol 2010;7(5):566–73.
[9] Compton BG, Gamble EA, Zok FW. Failure initiation during impact of metal spheres onto ceramic targets. Int J Impact Eng 2013;55:11–23.
[10] LaSalvia JC, McCauley JW. Inelastic Deformation Mechanisms and Damage in Structural Ceramics Subjected to High-Velocity Impact. Int J Appl Ceram Technol 2010;7(5):595–605.
[11] Sarva S, Nemat-Nasser S, Mcgee J, Isaacs J. The effect of thin membrane restraint on the ballistic performance of armor grade ceramic tiles. Int J Impact Eng 2007;34(2):277–302.
[12] S. D. Nunn, J. G. R. Hansen, B. J. Frame, and R. A. Lowden, "Improved ballistic performance by using a polymer matrix composite facing on boron carbide armor tiles," in *Advances in Ceramic Armor*, J. J. Swab Ed., Ceramic Engineering and Science Proceedings, D. Zhu and W. M. Kriven, Eds.: The American Ceramic Society, 2005, pp. 287-292.
[13] Reddy P, Madhu V, Ramanjaneyulu K, Bhat T, Jayaraman K, Gupta N. Influence of polymer restraint on ballistic performance of alumina ceramic tiles. Def Sci J 2008;58(2):264–74.
[14] Rahbek DB, Simons JW, Johnsen BB, Kobayashi T, Shockey DA. Effect of composite covering on ballistic fracture damage development in ceramic plates. Int J Impact Eng 2017;99:58–68.
[15] Oberg EK, Dean J, Clyne TW. Effect of inter-layer toughness in ballistic protection systems on absorption of projectile energy. Int J Impact Eng 2015;76:75–82.
[16] Crouch IG, Appleby-Thomas G, Hazell PJ. A study of the penetration behaviour of mild-steel-cored ammunition against boron carbide ceramic armours. Int J Impact Eng 2015;80:203–11.
[17] I. G. Crouch, "Effects of Cladding Ceramic and Its Influence on Ballistic," *28Th International Symposium on Ballistics, Vols 1 and 2*, pp. 1084-1094, 2014.
[18] Medvedovski E. Ballistic performance of armour ceramics: Influence of design and structure. Part 2. Ceram Int 2010;36(7):2117–27.
[19] Horsfall I, Buckley D. The effect of through-thickness cracks on the ballistic performance of ceramic armour systems. Int J Impact Eng 1996;18(3):309–18.
[20] Rahbek DB, Johnsen BB. Fragmentation of an armour piercing projectile after impact on composite covered alumina tiles. Int J Impact Eng 2019;133:103332.
[21] Jaitlee R. "Physical protection: Interdependence between hard armour and soft armour," Doctor of Philosophy (PhD). Melbourne, Australia: RMIT University; 2013.
[22] Zhikharev MV, Sapozhnikov SB, Kudryavtsev OA, Zhikharev VM. Effect of tensile preloading on the ballistic properties of GFRP. Composites Part B: Engineering; 2019.
[23] Tapie E, Tan ESL, Guo YB, Shim VPW. Effects of pre-tension and impact angle on penetration resistance of woven fabric. Int J Impact Eng 2017;106:171–90.
[24] Carton EP, Johnsen BB, Rahbek DB, Broos H, Snippe A. Round robin using the depth of penetration test method on an armour grade alumina. Defence Technology 2019;15(6):829–36.
[25] Børvik T, Dey S, Clausen AH. Perforation resistance of five different high-strength steel plates subjected to small-arms projectiles. Int J Impact Eng 2009;36(7):948–64.
[26] "AEP-2920: Edition A - Procedures for the evaluation and classification of personal armour - Bullet and fragmentation threats," ed: Nato Standardization Agency (NSA), 2014.
[27] "Ballistic Resistance of Body Armor NIJ Standard-0101.06," *NIJ Standard-0101.06*, ed. Washington DC, USA: U.S. Department of Justice, 2008.
[28] "AEP-55, Volume 1 (Edition 1) Procedures for the evaluating the protection level of logistic and light armoured vehicles," ed: Nato Standardization Agency (NSA), 2005.
[29] "MIL-STD-662F V50 Ballistic Test for Armor," ed: Department of Defense, United States of America, 1997.
[30] D. Mauchant, K. D. Rice, M. A. Riley, D. Leber, D. Samarov, and A. L. Forster, "Analysis of Three Different Regression Models to Estimate the Ballistic Performance of New and Environmentally Conditioned Body Armor," U.S. Department of Commerce, NISTIR 7760, 2011.
[31] Wright SC, Fleck NA, Stronge WJ. Ballistic Impact of Polycarbonate - An Experimental Investigation. Int J Impact Eng 1993;13(1):1–20.
[32] Kulkarni P, Mali KD, Singh S. An overview of the formation of fibre waviness and its effect on the mechanical performance of fibre reinforced polymer composites. Compos A Appl Sci Manuf 2020;137:106013.
[33] Russell BP, Karthikeyan K, Deshpande VS, Fleck NA. The high strain rate response of Ultra High Molecular-weight Polyethylene: From fibre to laminate. Int J Impact Eng 2013;60:1–9.
[34] Zhang R, Han B, Lu TJ. "Confinement effects on compressive and ballistic performance of ceramics: a review," presented at the. Int Mater Rev 2021.
[35] Hazell PJ, et al. On the improvement of the ballistic performance of a silicon carbide tile through pre-stress: Experiments and simulations. Int J Impact Eng 2021;151:103836.
[36] Sherman D. Impact failure mechanisms in alumina tiles on finite thickness support and the effect of confinement. Int J Impact Eng 2000;24(3):313–28.
[37] Elgy ID, Pickup IM, Gotts PL. Determination of the critical components of a complex personal armour rigid plate. In: Personal Armour Systems Symposium, Leeds, United Kingdom; 18-22 September 2006.